European Radiology (2019) 29:6266–6274
https://doi.org/10.1007/s00330-019-06255-z

HEAD AND NECK

Spectrally fat-suppressed coronal 2D TSE sequences may be more sensitive than 2D STIR for the detection of hyperintense optic nerve lesions

Tobias D. Faizy[1] · Gabriel Broocks[1] · Isabelle Frischmuth[1] · Carina Westermann[1] · Fabian Flottmann[1] · Michael H. Schönfeld[1] · Jawed Nawabi[1] · Hannes Leischner[1] · Daniel Kutzner[1] · Jan-Patrick Stellmann[2,3] · Christoph Heesen[2,3] · Jens Fiehler[1] · Susanne Gellißen[1] · Uta Hanning[1]

Received: 7 January 2019 / Revised: 16 April 2019 / Accepted: 25 April 2019 / Published online: 14 May 2019

Abstract

Objectives The aim of the study is to compare coronal spectrally fat-suppressed 2D turbo spin-echo (TSE) with 2D short-tau inversion-recovery (STIR) sequences for the detection of optic nerve hyperintensities in patients with acute optic nerve neuritis (ON).

Methods A retrospective review of patients with suspected unilateral ON and pathological visual evoked potentials, who received coronal TSE and STIR sequences with similar fast and clinically feasible acquisition times in addition to our standard imaging protocol. All images were evaluated and compared concerning the presence of optic nerve lesions, lesion lengths, and signal intensities in different anatomical parts of the optic nerves and CNR measures. A summary confidence score (CS) was calculated based on each reader's subjective confidence regarding the scoring items.

Results Interobserver agreements regarding the detection of optic nerve lesions were excellent for both sequences (TSE, $\kappa = 0.89$ and STIR, $\kappa = 0.80$). Greater extensions (17.4 ± 6.3 mm vs. 14.1 ± 5.8 mm), as well as higher numbers of optic nerve lesions in symptomatic nerves, were detected on TSE (49/52) compared with STIR (45/52) sequences (both $p < 0.001$). Overall CS were significantly ($p < 0.001$) higher for TSE (2.8) compared with STIR (2.1) sequences regarding the presence or absence of optic nerve lesions. CNR ratios of lesions' mean signal intensities vs. ipsilateral surrounding orbital fat and vs. signal intensity measurements from contralateral optic nerves were significantly higher on TSE compared with STIR ($p < 0.001$ for both comparisons).

Conclusion Spectrally fat-suppressed coronal 2D TSE sequences appear to be more sensitive for the detection of hyperintense optic lesions compared with 2D STIR sequences.

Key Points

- *Spectrally fat-suppressed TSE sequences showed higher detection rates of hyperintense optic nerve lesions, as well as a higher reader confidence scores compared with STIR.*
- *Optic nerve signal abnormalities on TSE sequences were brighter and showed a greater expansion along the optic nerve course.*
- *CNR measures were significantly higher on TSE compared with STIR, when comparing the ratios of mean signal intensities of optic nerve lesions to ipsilateral orbital fat and to contralateral healthy optic nerves of both sequences.*

Electronic supplementary material The online version of this article (https://doi.org/10.1007/s00330-019-06255-z) contains supplementary material, which is available to authorized users.

✉ Tobias D. Faizy
T.Faizy@uke.de

[1] Department of Diagnostic and Interventional Neuroradiology, University Medical Center Hamburg-Eppendorf, Martinistrasse 52, 20246 Hamburg-Eppendorf, Germany

[2] Institute of Neuroimmunology and Multiple Sclerosis, University Medical Center Hamburg-Eppendorf, Hamburg, Germany

[3] Department of Neurology, University Medical Center Hamburg-Eppendorf, Hamburg, Germany

Keywords Magnetic resonance imaging · Orbit · Multiple sclerosis: Optic nerve diseases · Neuromyelitis Optica

Abbreviations

AQP4-IgG	Aquaporin-4 immunoglobulin G
AU	Arbitrary unit
CHESS	Chemical shift selective
CIS	Clinically isolated syndrome
CS	Compound confidence score
CSF	Cerebrospinal fluid
IQR	Interquartile range
L-CON-Q	Lesion contralateral optic nerve quotient
MRI	Magnetic resonance imaging
MS	Multiple sclerosis
NMOSD	Neuromyelitis optica spectrum disorder
ON	Optic neuritis
PACS	Picture archiving and communication system
ROI	Region of interest
SE	Spin-echo
SPIR	Selective-partial inversion-recovery
STIR	Short-tau inversion-recovery
TSE	Turbo spin-echo
VEP	Visual evoked potentials
WM	White matter

Introduction

Optic nerve neuritis (ON) is the most common optic neuropathy, especially affecting young adults [1]. It is considered as an inflammatory demyelinating disorder of the optic nerve, which is strongly associated with chronic inflammatory CNS diseases, such as multiple sclerosis (MS) [2] or neuromyelitis optica spectrum disorders (NMOSD) [3], and is defined as a core criterion for the diagnosis of NMOSD (Table 1 in [4]). The diagnosis of ON is typically based on clinic aspects: patients present with reversible painful unilateral loss of vision in combination with abnormal visual evoked potentials (VEP) [5]. Nevertheless, clinical and laboratory assessments alone are not able to diagnose lesions' location and extension along the course of the optic nerve [6]. Therefore, MRI has gained an important role in the assessment of optic nerve lesions [6, 7]. For optic nerve imaging, coronal MRI techniques are broadly used and several studies have demonstrated the advantages of supplementary fat-suppression techniques [8–10]. Recent studies reported that the course of the optic nerve adjacent to fatty tissue may be best imaged using high-resolution, strongly T2-weighted fat-saturated spin-echo (SE) or inversion recovery sequences [6]. Consequently, the utilization of short-tau inversion-recovery (STIR) sequences is widespread [11], but other approaches using spectral fat presaturation may also be useful for the detection of ON [11, 12]. However, MRI-based evaluation of ON remains challenging, since the surrounding orbital fat may lead to high focal signal intensities and chemical shift artifacts may occur through perineural cerebrospinal fluid (CSF) [12]. Moreover, apart from a research environment, MRI sequences conducted in the clinical routine need to provide both clinically feasible acquisition times and sufficient diagnostic quality. To date, only a few studies exist evaluating the diagnostic findings of different fat suppression MRI techniques in patients with symptomatic ON. In this retrospective investigation, we conducted a clinical rater-based study to compare a strongly T2-weighted, spectrally fat-suppressed coronal 2D turbo spin-echo (TSE) sequence to the dedicated coronal 2D STIR sequence, both with similarly fast acquisition times. We assessed both sequences regarding the detectability of hyperintense optic nerve lesions, the assessability of anatomical localizations, investigators' confidence, and NMOSD-specific lesion criteria.

Methods

Patients' characteristics

The study was approved by the local research Ethical Committee following the guidelines of the Declaration of Helsinki and written informed consent was obtained from every subject.

From May 2015 to August 2018, 58 patients were referred to the Institute of Neuroimmunology with the suspicion of acute unilateral ON, confirmed by clinical findings of pathological visual evoked potentials and conclusive neuro-ophthalmological examination. All 58 patients underwent subsequent neuroimaging within 2 weeks after initial symptom onset and received coronal TSE and STIR sequences in addition to our standard protocol. As general inclusion criteria for our retrospective data analysis, we defined (1) patients with symptoms of acute ON, (2) ophthalmic examination prior to MRI with unilateral loss of vision in combination with abnormal visual evoked potentials (VEP), and (3) initial brain MRI imaging including additional coronal TSE and STIR sequences. Exclusion criteria were insufficient diagnostic image quality (e.g., due to motion artifacts). Six patients were excluded from our analysis, since optic nerve MRI images were not assessable. In 5 patients, bad image quality due to severe motion artifacts was detected on both sequences; in 1 patient considerable motion artifacts were detected on the STIR sequence only. Consequently, 52 patients were included in the present study.

Image acquisition parameters

Please refer to Supplementary Table 1.

Image analysis

Image quality and data processing

Sufficient image quality was ascertained by two experienced neuroradiologists prior to the reading and all images were assessed for interfering artifacts. After completion of the MRI scans, image data were transferred to the internal research picture archiving and communication system (PACS) and related patient data were anonymized simultaneously.

Standardized rating sheets

Supplementary Material 2 shows an example of a standardized rating sheet utilized for our investigation. Prior to image readings, a basic image-scoring training was performed by both readers based on 5 random patients, which were not included in our analysis.

Image data assessment

Image data of all enrolled patients were assessed in random order and readers were blinded to patients' identity and clinical symptoms. Two experienced neuroradiologists (7 and 8 years of experience) assessed all images on the same standard PACS workstation. Reader 1 first scored all STIR images and reader 2 scored all TSE images, respectively. After a delay of 10 days, both readers scored the other set of images accordingly. Lesion scoring was performed similar to the methodology described in [13]. In brief, for each patient, each optic nerve was assessed separately on TSE and STIR. Hyperintense optic nerve abnormality within the cross-sectional area of optic nerves was considered as a lesion. As proposed before [5], sole circumferential hyperintense signal abnormality of optic nerve sheaths was insufficient to be categorized as a lesion. The extent of optic nerve involvement was measured by assessing the number of consecutive images showing pathological hyperintensities and lesion length (in mm) calculated considering the slice thickness and intersection gaps of the sequences. Region of interest (ROI)–based mean relative lesion signal intensities, as well as corresponding signal intensities of the contralateral healthy-appearing optic nerves (on the same slices), were acquired. To compare the mean signal intensities between TSE and STIR sequences, additional ROI-based measurements were acquired from the ipsilateral frontal white matter (WM) of each patient and a ratio of mean relative lesion signal intensity to WM was calculated (lesion white matter quotient (L-WM-Q)) similar to [14]. To compare contrast measures (contrast-to-noise ratio (CNR)) between both sequences, two ROI-based signal intensity ratios were calculated: (1) hyperintense optic nerve lesion / adjacent ipsilateral orbital fat (mean of two ROIs at 1 and 7 o'clock position) (lesion orbital fat quotient (L-OF-Q)) and (2) hyperintense optic nerve lesion / contralateral optic nerve (lesion contralateral optic nerve quotient (L-CON-Q)). Optic nerve morphology was surveyed along with three distinct anatomical localizations: (1) intraorbital, (2) intracanalicular, and (3) intracranial (posterior part of the optic nerve including optic chiasm) as proposed in [6]. In case of disagreement and disputatious lesion assignment, a final consensus reading was performed by both readers.

Confidence rating

Following the approach described in [14], readers had to state their confidence level during image scoring based on a subjective grading system: (1) uncertain if abnormal, (2) possible abnormality, and (3) definite abnormality. To compare confidence ratings between the TSE and STIR sequences, a compound confidence score (CS) of subjective image ratings was calculated, as described in [14].

Statistical analysis

Univariable distribution of metric variables is described by median and interquartile range (IQR). For categorical data, absolute and relative frequencies are given. Interobserver reliability was assessed by computing Cohen's κ. Nonparametric Wilcoxon rank test was applied for comparisons of subjective confidence ratings (compound score). Paired t test was computed for comparisons of pathological imaging findings of optic nerves, i.e., comparisons of mean signal intensities of optic nerve lesions, lesion lengths, and CNR ratios between TSE and STIR images. Statistical significance for the results of hypothesis tests was corrected for multiple testing (Bonferroni correction) if applicable and assumed with an α-error of $p \leq 0.05$. For data analysis and spreadsheets, software packages SPSS (SPSS 24.0) and statistics in R version 3.2.2 were used.

Results

Baseline characteristics

Fifty-two patients (between May 2015 and August 2018) were enrolled in our study (13 male, 39 female). Median age was 34.3 ± 9.9 (interquartile range (IQR) 18–56). Until October 2018 (follow-up end for this study), all patients were reassessed clinically and by neuroimaging on a regular basis. Eleven patients were diagnosed with NMOSD based on the "International consensus diagnostic criteria for neuromyelitis

optica spectrum disorders" [4], of which 10 patients showed positive aquaporin-4 immunoglobulin G (AQP4-IgG) serum antibodies and one without proof of AQP4-IgG. During follow-up, 9 patients were diagnosed with clinically isolated syndrome (CIS) (i.e., patients showed typical early neurological symptom suspicious of MS at the time of study inclusion, but no definitive diagnosis of MS was made during follow-up [15]). Twenty-eight patients were diagnosed with relapsing-remitting MS (as indicated by ongoing relapses and proof of dissemination in time during follow-up), and 4 with secondary progressive MS (as indicated by progressive clinical worsening after 2 or more verifiable clinical relapses / 2 or more verifiable clinical lesions) based on the revised 2010 McDonald criteria [15].

Image quality

Subjectively, overall fat suppression was considered sufficient on both sequences. In 12 patients, artificial hyperintensities due to CSF flow-related artifacts were detected along the intracranial portion of the optic nerve on STIR images. In additional 8 patients, minor inhomogeneities of orbital fat were detected on STIR images in the intraorbital part of the optic nerve at the interfaces of air to bone. In 6 patients, minor CSF flow-related artifacts were present on TSE images along the intracranial part of the optic nerve. None of these artifacts impaired the diagnostic image quality with regard to the reading process.

Interobserver reliability

The overall interrater agreement concerning the presence or absence of hyperintense optic nerve lesions was excellent for both sequences ($\kappa = 0.89$ for TSE and $\kappa = 0.80$ for STIR). Rater CS was significantly higher regarding the detection of optical lesions on TSE compared to STIR sequences (TSE CS, 2.8 vs. STIR CS, 2.1; $p < 0.001$; z-score, − 5.28). Table 1 summarizes the results of the confidence rating of both readers.

Optic nerve lesion characteristics

After final consensus agreement, 45 hyperintense lesions were identified on STIR and 49 on TSE sequences ($p < 0.001$). In 3 patients, circumferential signal hyperintensities around the nerve sheaths of symptomatic nerves were present but were not considered as nerval abnormalities. No signal abnormalities were detected in asymptomatic nerves. Standardized mean signal intensities of optic nerve lesions differed significantly comparing TSE (L-WM-Q, 1.21 ± 0.19) to STIR (L-WM-Q, 0.98 ± 0.20) ($p < 0.001$, t-score, − 4.55). A greater extent of lesions (lesion length) was found on TSE (17.4 ± 6.3 mm) compared with STIR (14.1 ± 5.8 mm) images ($p = 0.001$). Regarding the CNR, the ratio of hyperintense optic nerve lesion to healthy adjacent orbital fat was significantly higher for the TSE (L-OF-Q, 4.41) compared with STIR (L-OF-Q, 3.21) ($p < 0.001$; t-score, − 4.12). The ratio of mean signal intensities of lesions to contralateral inconspicuous healthy optic nerves was significantly different between TSE (L-CON-Q, 2.31) and STIR (L-CON-Q, 1.57) ($p < 0.001$; t-score, − 3.89).

Assessability of anatomical localizations

Table 2 summarizes the findings of optic nerve lesions detected in different anatomical localizations. Of 49 optic nerve lesions detected on TSE images, 46 (98.9%) were located in the intraorbital, 34 (93.8%) in intracanalicular, and 14 (28.6%) in intracranial localizations. From a total number of 45 STIR optic nerve lesions, 39 (86.7%) appeared to be present intraorbital, 25 (55.6%) intracanalicular, and 14 (31.1%) intracranial. Overall CS, regarding the subjective assessability of anatomical localizations on both sequences, was higher for TSE compared with STIR sequences for intraorbital and intracanalicular, but not for intracranial localizations.

NMOSD-specific lesion characteristics

Table 3 displays imaging findings of readers' consensus scorings regarding NMOSD-specific optic lesion characteristics.

Table 1 Comparison of confidence ratings regarding the presence or absence of an optic lesion between TSE and STIR sequences

Sequence	Confidence rating			Compound score CS*
	Definite abnormality*, *n* (%)	Possible abnormality*, *n* (%)	Uncertain if abnormal, *n* (%)	
STIR	21 (46.7%)	23 (51.1%)	1 (2.2%)	2.1
TSE	41 (83.7%)	8 (16.3%)	0 (0%)	2.8

TSE, turbo spin-echo; *STIR*, short-tau inversion-recovery. Confidence ratings are displayed as percentage and compound score (CS, right column). Significant differences ($p \leq 0.05$) between the sequences are marked by an asterisk (*); 49 and 45 lesions were identified on TSE and STIR sequences, respectively. Non-parametric Wilcoxon rank test was applied for comparisons of subjective confidence ratings (compound score) between TSE and STIR sequences ($p < 0.001$; z-score, − 5.28)

Table 2 Summary of the findings of optic nerve signal abnormalities grouped by different anatomical localizations. Confidence ratings regarding the presence or absence of an optic nerve lesion are displayed as compound score (CS). Non-parametric Wilcoxon rank test was applied for comparisons of subjective confidence ratings (compound score) between TSE and STIR sequences. Significant differences ($p \leq 0.05$) between the sequences are marked by an asterisk (*). *TSE*, turbo spin-echo; *STIR*, short-tau inversion-recovery

Localization	STIR ($n = 45$)	TSE ($n = 49$)	CS STIR/TSE	p value	z-score
Intraorbital, n (%)	39 (86.7)	46 (98.9)	2.1/2.9	< 0.001*	− 6.01
Intracanalicular, n (%)	25 (55.6)	34 (93.8)	2.2/3.0	< 0.001*	− 6.42
Intracranial (including optic chiasm), n (%)	14 (28.6)	14 (28.6)	3.0/3.0	0.54	− 4.54

Summary of the findings of optic nerve signal abnormalities grouped by different anatomical localizations. Confidence ratings regarding the presence or absence of an optic nerve lesion are displayed as compound score (CS). Non-parametric Wilcoxon rank test was applied for comparisons of subjective confidence ratings (compound score) between TSE and STIR sequences. *TSE*, turbo spin-echo; *STIR*, short-tau inversion-recovery

No significant difference ($p = 0.41$) between TSE and STIR was detected regarding the presence of optic nerve lesions in the posterior parts including the optic chiasm. Lesions affecting more than half of the optic nerve length were detected more frequently on TSE compared with STIR ($p < 0.001$). From 11 patients diagnosed with NMOSD, NMOSD-specific lesion characteristics were fulfilled in 10 (90.9%) patients on TSE and 4 (36.4%) patients on STIR sequences ($p < 0.001$). CS, regarding NMOSD criteria, were high for both sequences and did not differ significantly (CS on TSE, 3.0 vs CS on STIR, 3.0 for all scoring items).

Discussion

In this retrospective rater-based study, we assessed hyperintense optic nerve lesions in patients with CIS, MS, and NMOSD, comparing coronal spectrally fat-suppressed TSE with conventional STIR sequences. We explored a superior diagnostic performance of TSE compared with conventional STIR sequences for the detection of optic nerve lesions in patients with acute ON. Lesions on TSE sequences exhibited significantly higher standardized signal intensities, higher CNR, and more extent optic nerve involvement and both readers stated a higher subjective scoring confidence when investigating lesions and anatomical landmarks on TSE sequences. Finally, in patients diagnosed with NMOSD, related optic nerve lesion characteristics [4] were fulfilled more conclusively on TSE compared with STIR sequences (Fig. 1). Our findings suggest that the utilization of TSE sequences for the detection of acute ON may be worthwhile for the clinical routine.

There are some dissimilarities between the TSE and STIR sequences, which may explain the different findings explored in our study. The beneficial effects of fat-suppression techniques, particularly in the context of ON, have been widely explored before [6, 12–14].

Technically, fat suppression on STIR images is achieved by the conduction of a 180° radio frequency pulse to invert the longitudinal magnetization as an initial excitation pulse in order to null fat signal. In contrast, as for the fat suppression of TSE sequences, the utilization of chemical shift selective (CHESS), short-duration radio frequency (RF) pulses are widely used [16]. Spectrally selective techniques employ a short-duration RF pulse tuned to the fat resonance frequency together with a spoiler gradient that saturates and dephases fat protons [17].

Table 3 Imaging findings regarding NMOSD-specific optic lesion characteristics and comparison of confidence ratings between TSE and STIR sequences

NMOSD criteria	STIR ($n = 45$)	TSE ($n = 49$)	p value	t-score	CS STIR/TSE	p value	z-score
Fulfillment of NMOSD-specific lesion characteristics	4 (8.9)	10 (20.4)	< 0.001	22,9	3.0 / 3.0	0.61	− 2.71
≥ half of optic nerve length	5 (11.1)	14 (28.6)	< 0.001	20	3.0 / 3.0	0.65	− 3.00
Posterior part of optic nerve (including optic chiasm)	14 (31.1)	14 (28.6)	0.41	24,7	3.0 / 3.0	0.88	− 2.53

Summary of the findings of optic lesion scoring regarding the neuromyelitis optica spectrum disease (NMOSD)–specific lesion criteria. Numbers in parenthesis in the top row display the number of all hyperintense lesions found in the specific sequence. Confidence ratings are displayed as compound score (CS). Non-parametric Wilcoxon rank test was applied for comparisons of subjective confidence ratings (compound score) between TSE and STIR sequences, but no significant differences were found regarding reader certainty between both sequences. Non-parametric Wilcoxon rank test was applied for comparisons of NMOSD-specific lesion criteria between both sequences. *TSE*, turbo spin-echo; *STIR*, short-tau inversion-recovery

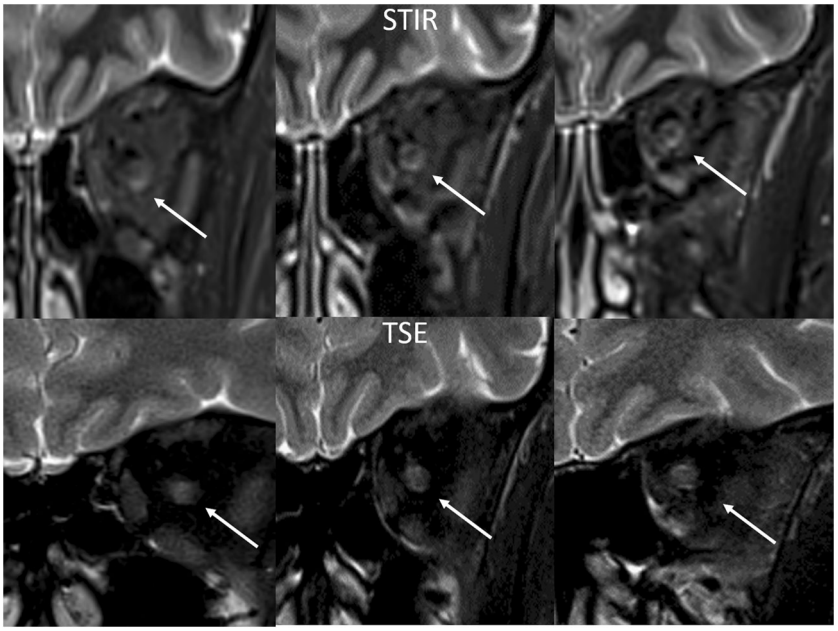

Fig. 1 Comparison of hyperintense optic nerve lesions between the TSE and STIR sequences. Exemplification of the diagnostic findings of TSE (lower three images) in comparison with STIR sequences (upper three images). Fat suppression seems to be more distinct on the TSE sequence, as the orbital fat appears strongly hypointense. White arrows indicate optic nerve lesions inside the left optic nerve. Confidence rating for lesions on TSE sequence was indicated as "possible abnormality," whereas optic nerve lesion on STIR was rated as "uncertain if abnormal"

The popularity of this method derives from the fact that it is easy to implement, generally effective and time-saving, and can be used in conjunction with any imaging sequence [18]. The major difference between both fat suppression techniques is that the conduction of inversion pulses is time-consuming and may result in elongated sequence TR at the expense of decreased image resolution. In contrast, the utilization of spectral fat suppression techniques may save valuable TR and thus signal, which may be used to enhance the spatial resolution of the conducted sequence. Consequently, when TSE and STIR sequences with similar acquisition times are being considered, TSE sequences can be performed with a better spatial resolution at the same amount of time. In accordance with previous reports [11–14], on the one hand, our results support the observation that higher spatial resolutions may result in improved detectability of optic nerve lesions and improved rater confidence. On the other hand, our results also suggest that the improved discriminability of lesions towards surrounding tissues or contralateral healthy nerves is also driven by higher CNR. Although the SNR of the used TSE is slightly lower compared with STIR, it appears that the interplay of improved spatial resolutions (smaller voxel sizes, similar FOV) and higher CNR is mainly responsible for the improved detection rates of optic nerve lesions in our investigation.

However, the utilization of STIR sequences is widespread for the detection of ON, due to their easy implementability on most MRI scanners and their relative robustness to magnetic field inhomogeneities [1, 13, 19]. In contrast, the major drawback of these useful sequences is the high signal intensities originating from CSF and loss of fat suppression is frequently observed within the orbits at air-bone interfaces [12]. Especially when shifting towards higher TEs, the proper discrimination of signal hyperintensities from CSF of perineural sheaths and optic nerve lesions remains challenging on STIR sequences [12, 14, 20]. Furthermore, any increase in proton density, T1 or T2, may result in an increase of signal intensities [14] and, therefore, the magnitude of true T2-weighting is comparatively low [14, 21, 22]. In contrast, strongly T2-weighted TSE sequences may be more suitable for the detection of edema-like T2 components within cross-section of optic nerves that are widely found in patients with ON [6, 23], since these techniques provide homogeneous fat suppressions, better CNR, and mostly ignore the effect of additive T1/T2 contrast present on STIR (Fig. 2). However, the resultant lower SNR in other brain parts may restrict the use of highly T2-weighted TSE sequences for the simultaneous evaluation of other structural abnormalities, such as demyelinating brain plaques (dotted arrows on Fig. 3), since they may be "disguised" and difficult to detect.

Noteworthy, an improved detectability of optic nerve lesions has also been demonstrated for other related hybrid imaging techniques, such as selective-partial inversion recovery (SPIR) [2, 14, 21]. SPIR sequences utilize additional spectral presaturation in combination with inversion pulses to null fat. Compared with STIR, this approach also results in considerable increases of spatial resolutions [14] and thus in increased ratios of signal intensities between neuritic and non-neuritic nerve segments [20], comparable to the findings on TSE sequences in our study. However, this effect becomes even more distinct,

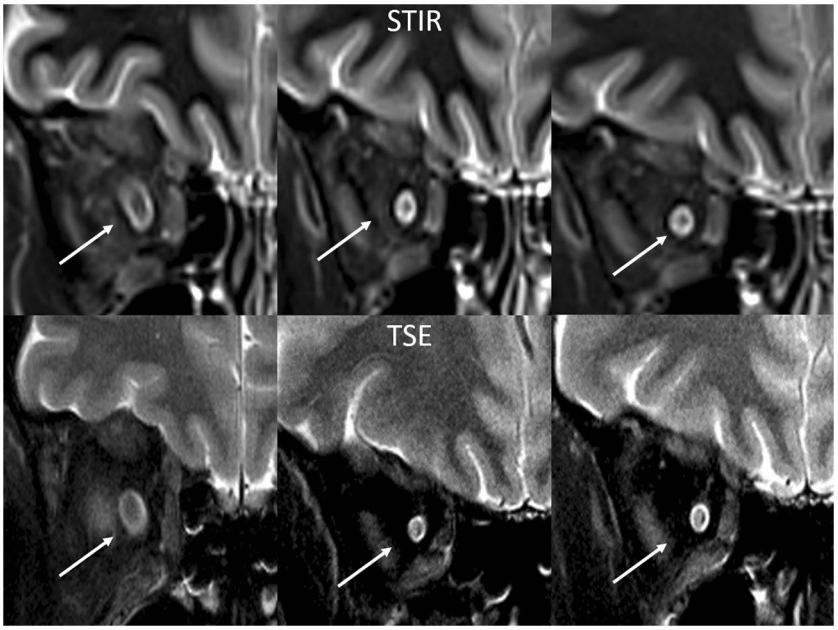

Fig. 2 Hyperintense optic nerve lesions in a patient with NMOSD. A displayed comparison of hyperintense optic nerve lesions detected on the TSE (lower three images) and the STIR sequence (upper three images) in a patient who was diagnosed with NMOSD (positive AQP4-IgG). Both sequences show considerable signal hyperintensities derived from CSF of the optic nerve sheath. White arrows indicate the same optic nerve lesion on both sequences. The optic nerve lesion on the TSE sequence was regarded as definite abnormality, whereas the lesion on STIR was indicated as possible abnormality

when additional suppression of water signals is induced (SPIR-FLAIR), due to the absence of signal intensity from perineural CSF [20]. However, compared with TSE, acquisition times of SPIR/SPIR-FLAIR sequences are considerably longer (TSE, ~2 min vs. SPIR-FLAIR, 4 min and 25 s in [14]), restricting its use for the clinical routine and making it more prone to movement artifacts due to longer scan times. Moreover, especially when shifting towards higher TEs, the proper discrimination of signal hyperintensities from CSF of perineural sheaths and nerve lesions remains challenging on SPIR sequences [12, 14, 20].

In our investigation, NMOSD-specific MRI lesion criteria of optic nerve involvement were fulfilled more conclusively on TSE. Although the diagnosis of chronic inflammatory diseases, such as MS or NMOSD, ultimately requires confirmation through clinical laboratory tests, many studies reported of the potential usefulness of suitable MRI sequences for the evaluation of the extent of hyperintense optic nerve lesions in terms of prognostic implications of these diseases [3, 4, 6,

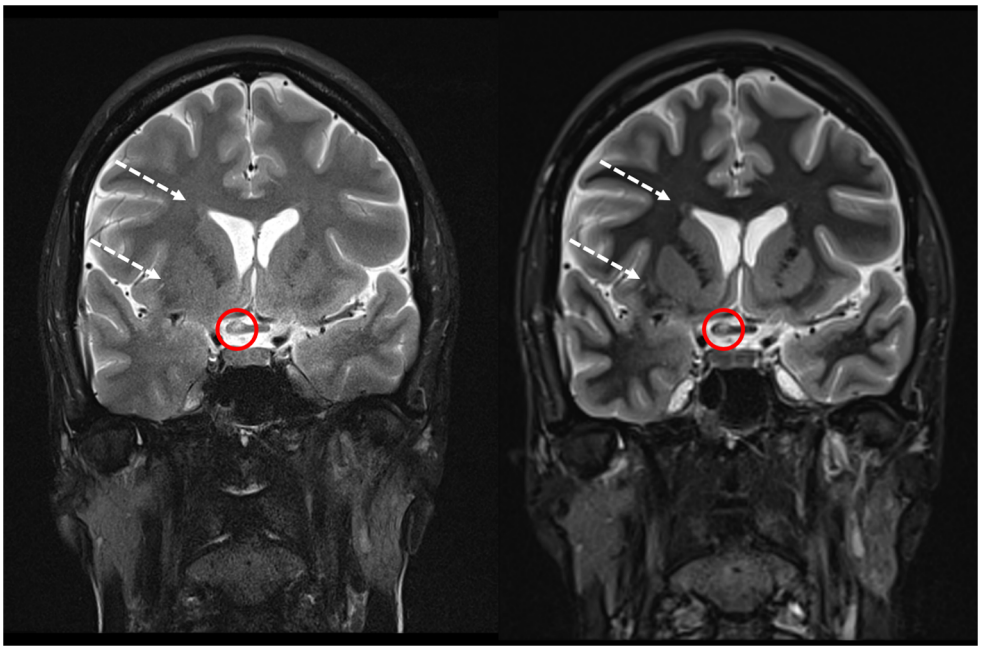

Fig. 3 Comparison of hyperintense optic nerve lesion inside the optic chiasm. Comparison of TSE (left side) vs. STIR (right side) images on the level of optic chiasm. Red circles indicate a hyperintense optic nerve lesion inside the optic chiasm of an NMOSD patient. Both readers referred to the lesion as definite abnormality. Dotted arrows indicate two demyelinating white matter lesions, hardly detectable on TSE sequences

12]. Noteworthy, compared with STIR, lesions on TSE showed considerably higher signal intensities. In accordance with previous findings [14], this may be another explanation for improved lesion detection rates on TSE along the course of the optic nerve.

Our study holds some limitations. This retrospective study was designed to compare two established and broadly available MRI sequences with different types of fat-suppression techniques within similar acquisition times. We are aware of the fact that there are vast possibilities to adjust scan parameters, image resolutions, and acquisition times to modify image quality. We acknowledge that an increase of scan time most likely would result in an improvement of image quality; however, this is not a scope of this manuscript. Moreover, readers' lesion and confidence scorings are subjective by nature and therefore, we must stress a general subjectivity bias and a bias resulting from readers suspicion towards the expected imaging findings during the scoring process. Moreover, the diagnosis of NMOSD primarily is based on a conjunction of clinical laboratory parameters and we would like to clearly point out that findings of optic nerve MRI are only a minor contributor to the final diagnosis. Since no histopathological data was included, all claims about the specificity of optic nerve lesions must be mitigated.

Conclusion

Highly T2-weighted and spectrally fat-suppressed coronal TSE sequences appear to be a useful tool for the detection of optic nerve signal abnormalities, exhibiting considerably higher spatial resolutions, as well as superior delineation of optic nerve lesions and subjective rater confidence due to higher CNR compared with STIR sequences with similar acquisition times.

Funding The authors state that this work has not received any funding.

Compliance with ethical standards

Guarantor The scientific guarantor of this publication is Professor Dr. med. Jens Fiehler, Hamburg.

Conflict of interest The authors of this manuscript declare no relationships with any companies whose products or services may be related to the subject matter of the article.

Dr. Stellmann reports grants from Alpina, during the conduct of the study; grants and personal fees from Biogen; personal fees from Genzyme; and grants from Novartis, outside the submitted work. These fundings did not compromise or influence the scientific work presented in this manuscript.

Statistics and biometry Dr. Uta Hanning and Dr. Fabian Flottmann have significant statistical expertise. No complex statistical methods were necessary for this paper.

Informed consent The study was approved by the local research Ethical Committee Hamburg (Ethik-Komission der Ärztekammer Hamburg), following the guidelines of the Declaration of Helsinki and written informed consent was given from every participant.

Ethical approval Institutional Review Board approval was obtained.

Methodology
- Retrospective
- Diagnostic or prognostic study
- Performed at one institution

References

1. Toosy AT, Mason DF, Miller DH (2014) Optic neuritis. Lancet Neurol 13:83–99
2. Wilhelm H, Schabet M (2015) The diagnosis and treatment of optic neuritis. Dtsch Arztebl Int 112:616–625 quiz 626
3. Dutra BG, da Rocha AJ, Nunes RH, Maia ACM Júnior (2018) Neuromyelitis optica spectrum disorders: spectrum of MR imaging findings and their differential diagnosis. Radiographics 38:169–193
4. Wingerchuk DM, Banwell B, Bennett JL et al (2015) International consensus diagnostic criteria for neuromyelitis optica spectrum disorders. Neurology 85:177–189
5. Hickman SJ, Miszkiel KA, Plant GT, Miller DH (2005) The optic nerve sheath on MRI in acute optic neuritis. Neuroradiology 47:51–55
6. Becker M, Masterson K, Delavelle J, Viallon M, Vargas MI, Becker CD (2010) Imaging of the optic nerve. Eur J Radiol 74:299–313
7. Jenkins TM, Toosy AT (2017) Optic neuritis: the eye as a window to the brain. Curr Opin Neurol 30:61–66
8. Guy J, Mao J, Bidgood WD Jr, Mancuso A, Quisling RG (1992) Enhancement and demyelination of the intraorbital optic nerve. Fat suppression magnetic resonance imaging. Ophthalmology 99:713–719
9. Hendrix LE, Kneeland JB, Haughton VM et al (1990) MR imaging of optic nerve lesions: value of gadopentetate dimeglumine and fat-suppression technique. AJR Am J Roentgenol 155:849–854
10. Johnson G, Miller DH, MacManus D et al (1987) STIR sequences in NMR imaging of the optic nerve. Neuroradiology 29:238–245
11. Onodera M, Yama N, Hashimoto M et al (2016) The signal intensity ratio of the optic nerve to ipsilateral frontal white matter is of value in the diagnosis of acute optic neuritis. Eur Radiol 26:2640–2645
12. Hodel J, Outteryck O, Bocher AL et al (2014) Comparison of 3D double inversion recovery and 2D STIR FLAIR MR sequences for the imaging of optic neuritis: pilot study. Eur Radiol 24:3069–3075
13. Riederer I, Mühlau M, Hoshi MM, Zimmer C, Kleine JF (2019) Detecting optic nerve lesions in clinically isolated syndrome and multiple sclerosis: double-inversion recovery magnetic resonance imaging in comparison with visually evoked potentials. J Neurol 266:148–156
14. Jackson A, Sheppard S, Laitt RD, Kassner A, Moriarty D (1998) Optic neuritis: MR imaging with combined fat- and water-suppression techniques. Radiology 206:57–63
15. Polman CH, Reingold SC, Banwell B et al (2011) Diagnostic criteria for multiple sclerosis: 2010 revisions to the McDonald criteria. Ann Neurol 69:292–302
16. Siewert C, Hosten N, Felix R (1994) The use of the T2-weighted turbo-spin-echo sequence in studying the neurocranium. A comparison with the conventional T2-weighted spin-echo sequence. Rofo 161:44–50

17. de Kerviler E, Leroy-Willig A, Clément O, Frija J (1998) Fat suppression techniques in MRI: an update. Biomed Pharmacother 52: 69–75
18. Keller PJ, Hunter WW Jr, Schmalbrock P (1987) Multisection fat-water imaging with chemical shift selective presaturation. Radiology 164:539–541
19. Naganawa S, Koshikawa T, Nakamura T et al (2004) Comparison of flow artifacts between 2D-FLAIR and 3D-FLAIR sequences at 3 T. Eur Radiol 14:1901–1908
20. Aiken AH, Mukherjee P, Green AJ, Glastonbury CM (2011) MR imaging of optic neuropathy with extended echo-train acquisition fluid-attenuated inversion recovery. AJNR Am J Neuroradiol 32: 301–305
21. Onofrj M, Tartaro A, Thomas A et al (1996) Long echo time STIR sequence MRI of optic nerves in optic neuritis. Neuroradiology 38: 66–69
22. Tartaro A, Onofrj M, Delli Pizzi C et al (1996) Long time echo STIR sequence magnetic resonance imaging of optic nerves in optic neuritis. Ital J Neurol Sci 17:35–42
23. Voss E, Raab P, Trebst C, Stangel M (2011) Clinical approach to optic neuritis: pitfalls, red flags and differential diagnosis. Ther Adv Neurol Disord 4:123–134